Section 2
PROGRESS IN LASER FUSION

2.A Numerical Simulation of Recent, 24-Beam, Blue (351-nm) OMEGA Implosion Experiments

LLE is presently involved in a series of experiments intended to demonstrate the ability of direct-drive laser fusion to ablatively compress microencapsulated deuterium-tritium (DT) fuel to 200 times its liquid density. This campaign has been structured into three parts. The first part was initiated in February 1985 and involved the implosion of glass microballoons filled with various pressures of DT gas. Compression of these initial targets attained maximum fuel densities of 6.0 to 6.5 g/cm^3, or ~30 times liquid DT density (30 XLD) and maximum neutron yields in the range of 1.5 to 2.0 × 10^{11}. The experiments also served to test recently added diagnostics on the OMEGA system which will be necessary to evaluate the final 200-XLD targets. These diagnostics include knock-on fuel ion spectrometry for measuring fuel areal density ($<\rho R>$),[1] radiation chemistry techniques (RAD-CHEM) for measuring shell areal densities ($<\rho\Delta R>$),[2] neutron time-of-flight equipment for determining core temperatures,[3] and Kirkpatrick-Baez (K-B) microscopes, which give spatially resolved x-ray emission information from the imploding shell.[4]

The second phase of the 200-XLD campaign is to begin in January 1986. Because of the unavailability of cryogenic targets, this phase will involve the use of targets similar to those in the first phase, and high-pressure (100- to 150-atm), DT-filled glass microballoons. One-dimensional simulations show that the implosion characteristics (e.g., convergence ratios) of small-diameter, high-pressure targets resemble those of targets using moderately thick layers of cryogenic fuel. As such, these "surrogate cryogenic" targets will provide preliminary information concerning the implosion of cryogenic targets. Furthermore, because the small diameters of these targets will result in high illumination intensities (i.e., $>2 \times 10^{15}$ W/cm^2), these targets might provide experimental data reflecting the presence of certain plasma physics processes (e.g., $2\omega_p$, self-focusing, etc.) in the underdense corona. Finally, should the fabrication of bare plastic shells containing thick layers of cryogenic DT fuel prove difficult, these high-pressure, glass-shell targets will be frozen and used in the final phase of the 200-XLD campaign.

The third and final stage of the 200-XLD campaign, expected to be initiated in the summer of 1986, involves the use of cryogenic DT fuel overcoated with plastic shells. It is through the compression of these cryogenic targets that the expected goal of fuel densities in excess of 200 XLD is to be achieved.

This article presents comparisons between numerical simulations (both one- and two-dimensional) and recent experimental results obtained from the initial phase of the 200-XLD campaign on the OMEGA system. The numerical simulations were carried out using the one-dimensional hydrodynamics code, *LILAC*,[5] and the two-dimensional hydrodynamics code, *ORCHID*. Both codes, which were developed at the University of Rochester, are based on a one-fluid, two-temperature approximation employing the use of Lagrangian hydrodynamics. The calculations include (1) tabular equation of state (SESAME[6]), (2) flux-limited electron thermal transport,[7] (3) multifrequency-group radiation transport using LTE opacities reduced from the LANL Astrophysical Library,[8] and (4) the use of geometrical optics ray tracing[9] for the deposition of laser energy by inverse bremsstrahlung. Emphasis is placed on comparison between experiment and simulation in neutron yields, fuel and shell areal densities, and x-ray emission images.

Fig. 25.6
2.0-kJ generic target designs used for attaining (a) high yield and (b) high density. Both designs call for initial fuel pressures of 10 atm.

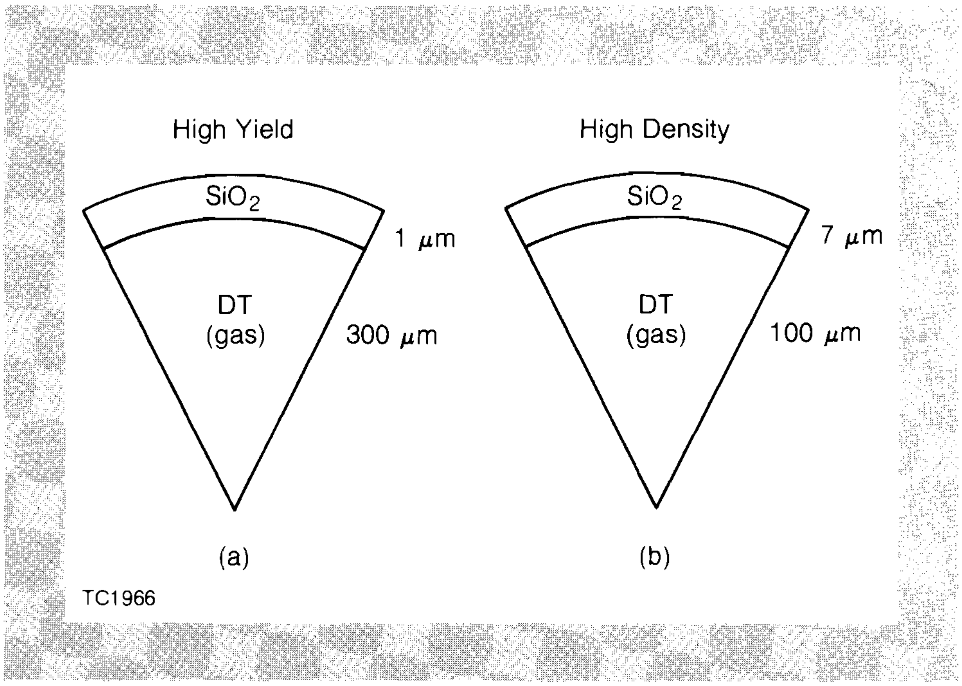

Target Design Overview

Preliminary scoping studies[10] were performed to identify candidate target designs for use in the initial phase of the 200-XLD campaign. The two basic designs that emerged from this work are shown in Fig. 25.6. The first of these designs [Fig. 25.6(a)] is intended to maximize neutron yield. Optimal performance of such targets requires that the target shell be accelerated to high velocities that will, upon stagnation at the center of the pellet, produce high core temperatures. Therefore, these targets have large initial diameters that maximize the absorbed laser energy and use thin (low-mass) shells to maximize the resulting shell velocity. The simulated behavior is represented in Fig. 25.7.

Viewing the radius versus time (R-T) plot shown in Fig. 25.7(a), it should first be noted that this target is being driven ablatively rather than explosively. In an exploding pusher, the shell blows apart, with roughly half the mass moving out and the other half moving toward the center. In an R-T plot for such an implosion, the half-mass point within the shell (approximately the shell midpoint) would remain relatively motionless until after the imploding part of the shell rebounds. For ablatively driven targets, the driving force is not generated at the shell midpoint but at the ablation surface near the outer edge of the shell. As such, the ablation process "peels away" the outer layers of the shell while accelerating the remaining mass inward. Although most of the shell mass is initially accelerated inward, less than half remains by the time the shell reaches stagnation. Neither the mass of the imploding shell nor the position of the shell midpoint remains constant during the implosion for ablatively driven targets.

One-dimensional simulations show that the glass-fuel interface velocity, illustrated in Fig. 25.7(b), easily exceeds 4×10^7 cm/s, and in some cases approaches 6×10^7 cm/s. These high-velocity shells produce high core temperatures as a result of shock heating and shell stagnation. The simulated neutron energy spectrum is shown in Fig. 25.7(c). Applying the prescription put forth by Brysk,[3] the neutron-averaged ion temperature for this implosion was $\sim$5.0 keV. The neutron spectrum was integrated and gave a neutron yield of $\sim 1.60 \times 10^{12}$ neutrons. Both of these results are consistent with results from the overall simulation. Although such yields are quite encouraging, the corresponding maximum densities are low. The temporal density profile is displayed in Fig. 25.7(d), showing a maximum fuel density of only 0.89 gm/cm^3, corresponding to $\sim$ 4 XLD.

The second type of design [Fig. 25.6(b)] is intended to maximize the compressed fuel density. This type of target requires that increases in the fuel temperature due to nonisentropic processes (e.g., shock preheat) be kept as low as possible, providing a relatively massive inward-moving shell with minimal resistance in compressing the fuel to high densities. These targets require the use of small diameters to limit the distance over which the acceleration can act, and of relatively thick shells to lower implosion velocities. The simulated behavior is shown in Fig. 25.8.

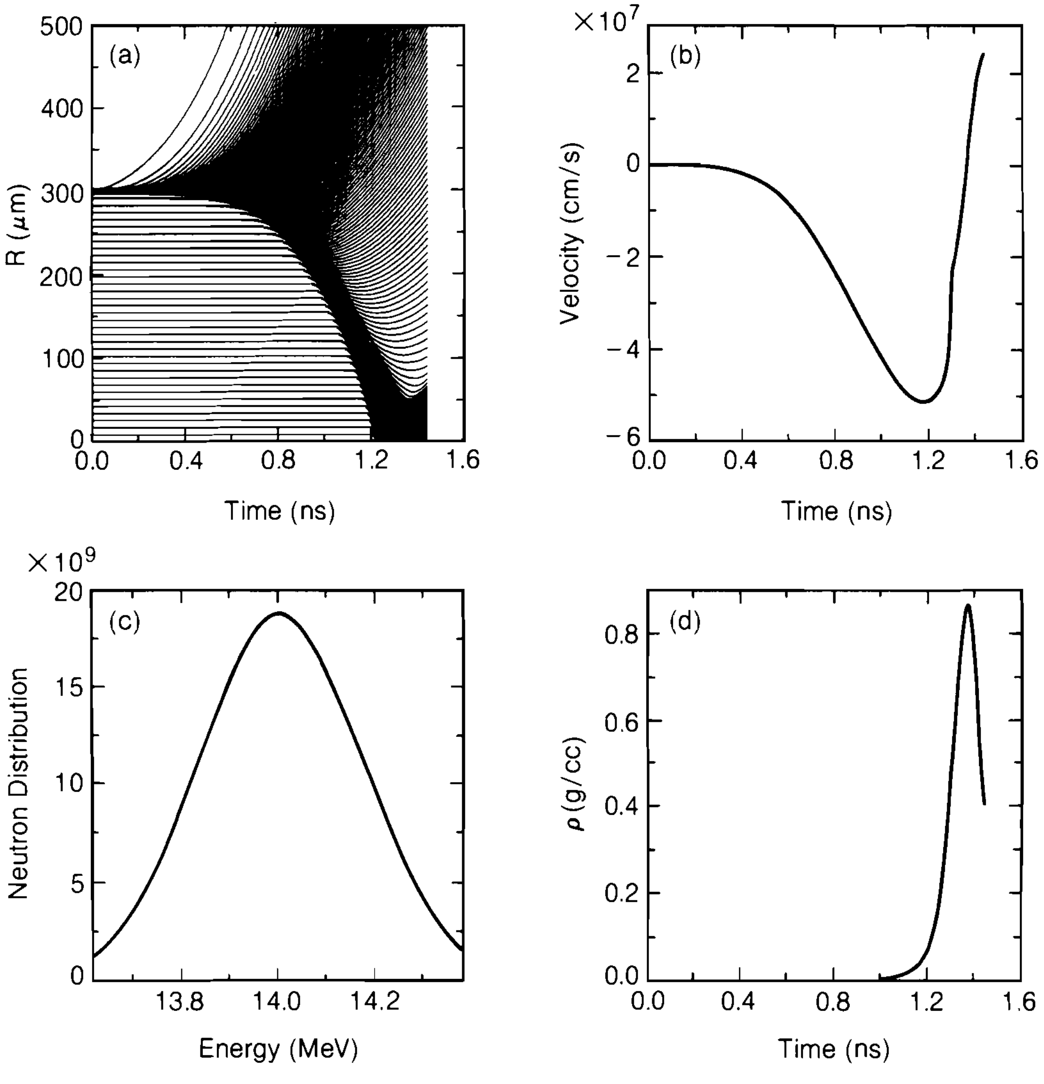

TC1967

Fig. 25.7
One-dimensional LILAC *simulation of a high-yield target:*
(a) R-T plot,
(b) interface velocity history,
(c) neutron energy spectrum, and
(d) fuel density history.

As before, the R-T plot [Fig. 25.8(a)] shows that this target is being ablatively driven. An additional feature is that a slight shock breaks out of the interior surface of the glass shell because of the lower velocity achieved by these targets. The lower velocities [between 1 and 2 × 10^7 cm/s, shown in Fig. 25.8(b)] produce only modest temperatures (1–2 keV), allowing the incoming shell to compress the fuel on a much lower adiabat to high densities. The analysis of the predicted neutron energy spectrum [Fig. 25.8(c)] illustrates the generation of only modest temperatures. This spectrum shows the neutron-averaged temperature to be ~ 1.6 keV and the neutron yield to be 1.00 × 10^{10}. Because of the low temperatures, the maximum fuel density predicted [Fig. 25.8(d)] is 45 g/cm^3, or 210 XLD.

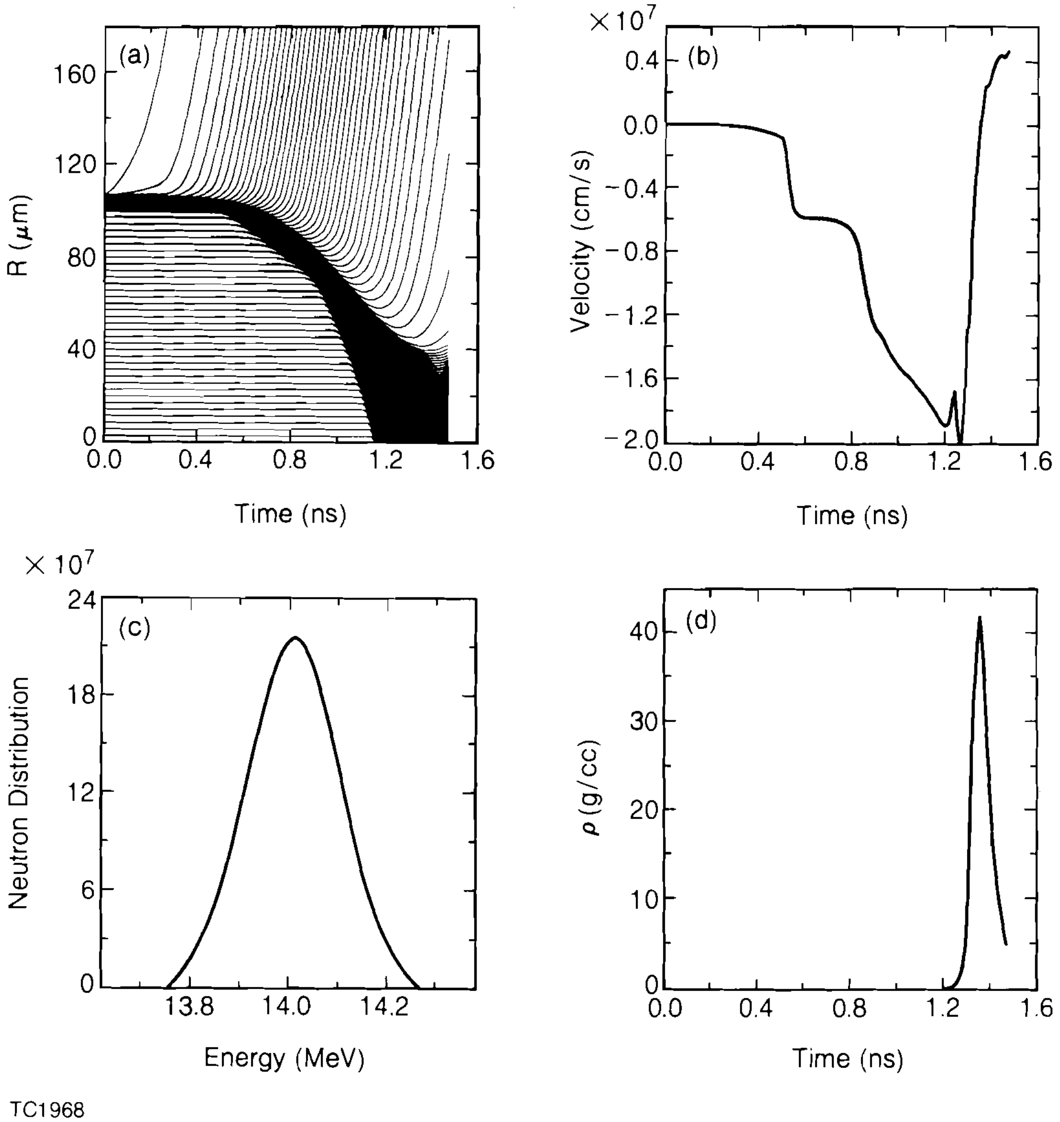

Fig. 25.8
One-dimensional LILAC *simulation of a high-density target:*
(a) R-T plot,
(b) interface velocity history,
(c) neutron energy spectrum, and
(d) fuel density history.

In summary, the targets used for the initial phase of the 200-XLD campaign fell into two categories. The first, high yield, was necessary to provide neutrons for testing new diagnostics to be used in the analysis of the final 200-XLD cryogenic target implosions. The other category, high density, was designed to maximize fuel density and provides an initial setting from which the final goal of 200 XLD can be achieved.

Experimental Comparison

The initial sequence of experimental implosions on the 24-beam, blue (351-nm), 2-kJ OMEGA laser system was completed in June 1985.[11] In conjunction, there was a significant numerical-simulation campaign, in both one and two dimensions, designed to provide additional insight into the interpretation of the experimental results. Particular interest has been paid to the comparison of overall neutron yields, fuel and shell areal densities, and x-ray microscope film response curves.

The comparison between experimental and predicted neutron yields has traditionally been displayed as a function of the initial glass shell thickness. When applied to the large number of significantly different target designs involving different initial aspect ratios, initial fill pressures, and the occasional use of plastic overcoats, however, this relationship failed to provide any useful insight into this series of implosions. A more meaningful display of the comparison between the experimental and predicted neutron yield was found in terms of the one-dimensional predicted convergence ratio. (Here the convergence ratio is defined as the ratio of the initial fuel radius divided by the fuel radius of the stagnated core.) This relationship was further simplified by normalizing the experimental yields to the corresponding one-dimensional prediction. Results are shown in Fig. 25.9.

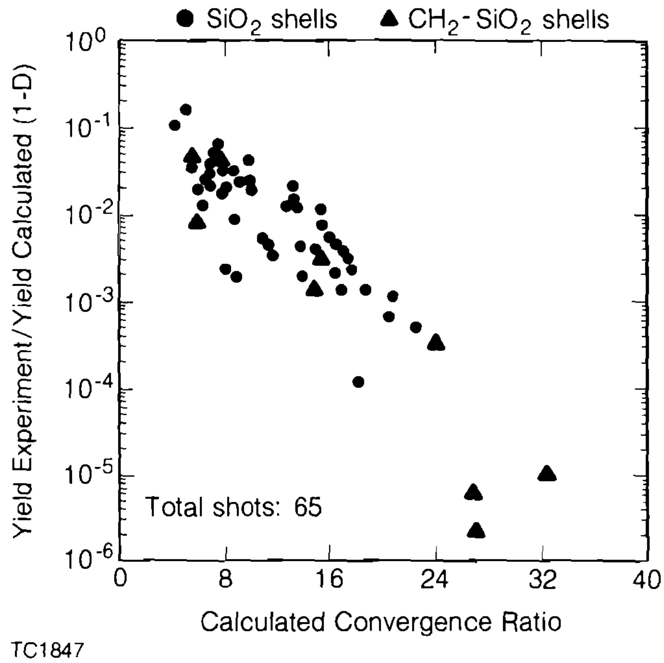

Fig. 25.9
Experimental neutron yields, normalized to the calculated one-dimensional yield, drawn as a function of the calculated convergence ratio.

In Fig. 25.9, the strong dependence of the normalized neutron yield on the predicted convergence ratio is clearly evident. This graph shows that experiments with targets requiring high predicted convergence ratios (i.e., 15–30) performed very poorly in comparison with one-dimensional simulations. The declining agreement with increased predicted convergence ratio suggests the possible presence of implosion nonuniformities. The presence of these nonuniformities would be expected to disrupt the compressed core and prematurely terminate the thermonuclear burn. As a result, the neutron-weighted diagnostics (i.e., knock-on ion spectrometry and RAD-CHEM techniques) would give physical information that no longer corresponds to the time of peak compression but rather to an earlier time corresponding with the termination of burn. In Fig. 25.10, the measured fuel and shell areal densities are compared with the areal densities at those times in the simulations when the neutron yields equal the total experimental yields. At these points in the implosions, Fig. 25.10(a) shows agreement between the experimental and simulated fuel $<\rho R>$ values over the range of predicted convergence ratios. However, the shell $<\rho R>$ comparison, illustrated in Fig. 25.10(b), shows that the experiments achieve higher values than the simulations as the convergence ratio is increased. The different behavior of the fuel and shell areal-density comparisons can again be explained by the existence of nonuniformities in the target. At this point in the implosion, the fuel $<\rho R>$ is dominated by volume changes in the core due to the imploding shell. Although the shell is deformed, the difference in volumes between the perturbed and unperturbed cases is small and, as such, the experimental and simulated fuel $<\rho R>$ values should be in agreement. The shell $<\rho \Delta R>$ values, however, are very sensitive to distortions in the shell. Because deformations in the shell cause increased compression, the measured shell $<\rho \Delta R>$ values would be higher than those predicted by the simulation. It is important to point out, therefore, that attempts to infer core conditions (e.g., fuel density) from the measured shell areal density can give incorrect results if care is not taken to analyze the entire implosion.

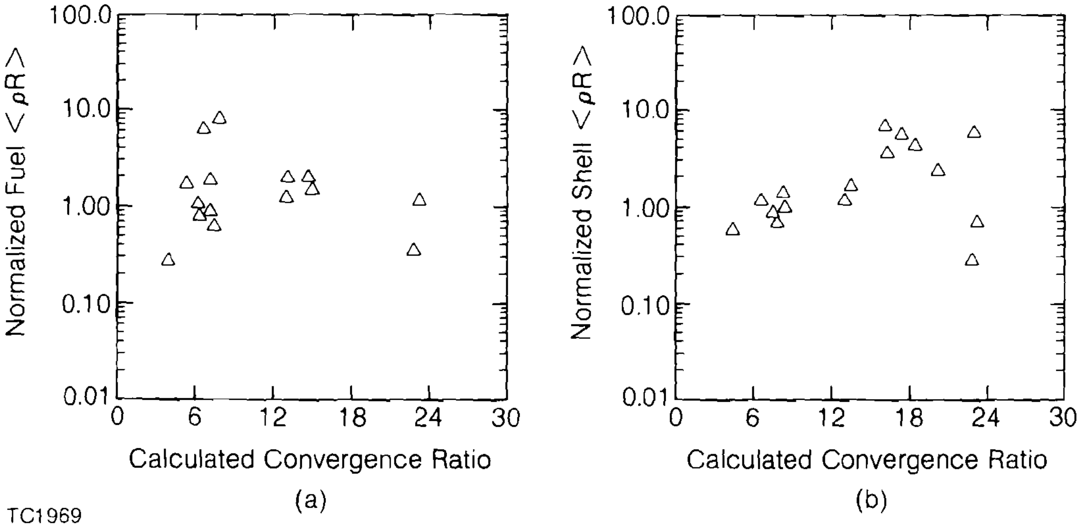

(a) (b)

Fig. 25.10
Experimental fuel (a) and shell (b) areal densities, normalized to calculated one-dimensional results, drawn as a function of the calculated convergence ratio.

Further evidence of the existence of nonuniformities is provided by the analysis of K-B microscope images taken from a series of implosion experiments on comparable targets, each illuminated at a different focal position. Since the level of illumination nonuniformity increases with decreasing focal position,[12] experimental agreement with one-dimensional predictions should become poorer as the focal position is decreased. Comparing the azimuthally averaged film density profile of a K-B microscope image and the corresponding time-integrated profile predicted by *LILAC*, as shown in Fig. 25.11(a), it is possible to determine an average core radius from both the experiment and the simulation. The ratio of the measured core radius to the predicted core radius, versus initial focal position for these targets, is illustrated in Fig. 25.11(b). It can be seen that the agreement between experiment and simulation becomes poorer as the focal position is reduced from 8R (good illumination uniformity) to 2R (poor illumination uniformity).

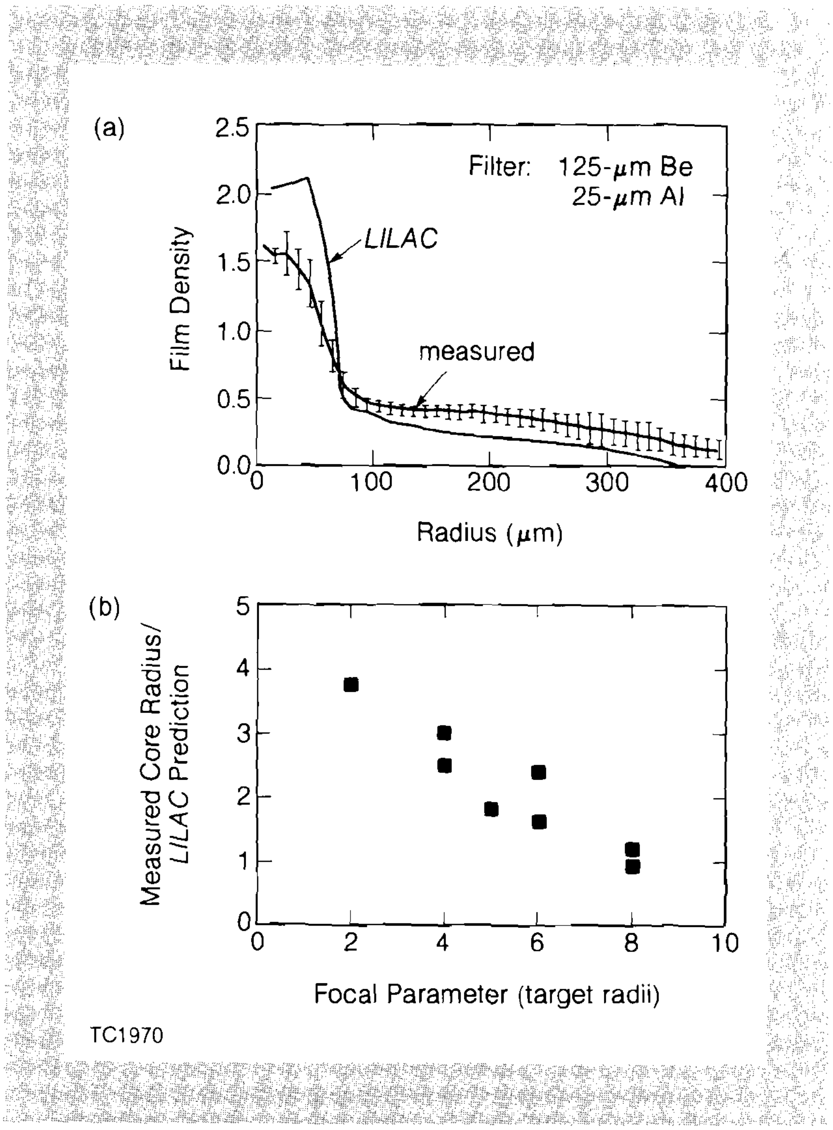

Fig. 25.11
X-ray micrograph profiles:
(a) emission comparison between experiment and simulation for shot No. 11309,
(b) ratio of averaged core radii (experimental divided by simulated) drawn as a function of initial focal position.

Illumination Nonuniformities

In attempting to understand the effects of the nonuniformities on target performance, it is first necessary to identify the source of the nonuniformities on target. The analysis of the nonuniformities originating from the laser illumination is complex and difficult. Contributions to the illumination nonuniformities can come from several sources, including (1) number of beams, (2) individual beam profile, (3) focal position, (4) energy balance between beams, and (5) beam placement on target.

All of these elements have been incorporated into a computer simulation[12] which decomposes the resulting illumination nonuniformity into its individual spherical harmonics to determine the characteristic spatial wavelengths. Using a typical beam profile from the OMEGA system during the first phase of the 200-XLD campaign, the resultant irradiation pattern was decomposed into its spherical harmonics for various focal positions. The total illumination nonuniformity, as a function of focal position, is shown in Fig. 25.12. The contribution of each individual spherical harmonic (ℓ-mode) to the total nonuniformity for a 6R focus is shown in Fig. 25.13.

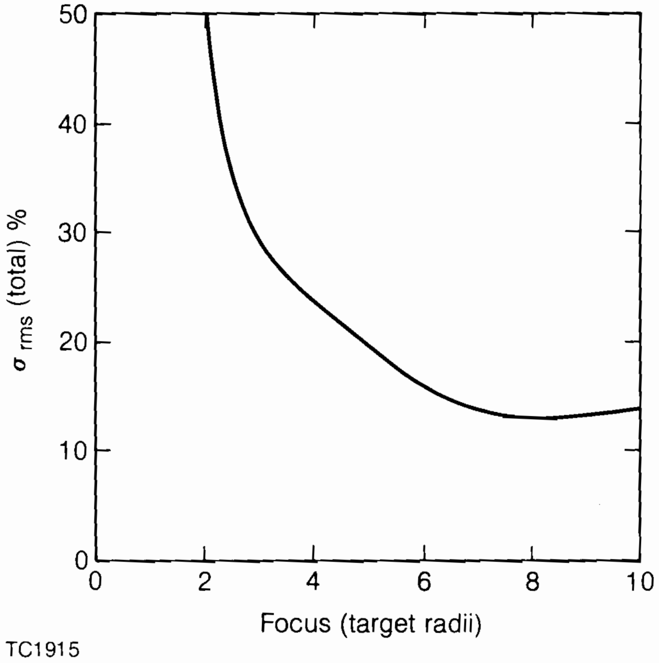

Fig. 25.12
Levels of illumination nonuniformities versus focal position for current OMEGA system.

Once the magnitude and wavelength of the illumination nonuniformity have been identified, they can be incorporated into the two-dimensional hydrodynamics code, *ORCHID*, to determine the effect on performance of an individual target. However, due to limitations in computer resources, it is not possible to simulate the entire illumination nonuniformity. For the nonuniformity spectrum shown in Fig. 25.13, only the ℓ = 2, 4, and 8 contributions, which account for 75% of the total nonuniformity, were used in the simulation. These three modes were combined in phase (producing approximately a 50% peak-to-valley variation characteristic of the calculated nonuniformity), and the resultant nonuniformity was superimposed on normal incident irradiation in the *ORCHID* simulation.

The experiment simulated by *ORCHID* was shot No. 11233, which produced the second-highest neutron yield (1.62×10^{11}) in this implosion series. The *ORCHID* simulation predicted a neutron yield of 5.12×10^{11}, while the one-dimensional simulation gave a yield of

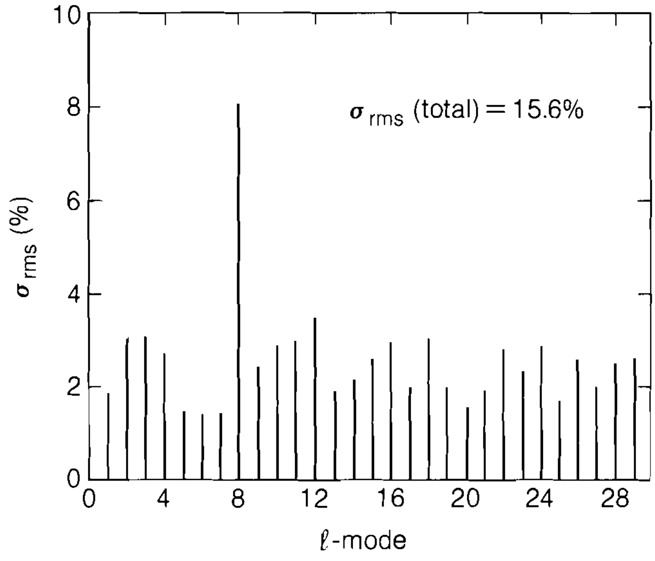

Fig. 25.13
Modal structure of illumination nonuniformity for current OMEGA system at 6R focusing.

2.33×10^{12} neutrons with maximum neutron-averaged fuel and shell areal densities of 2.51×10^{-3} g/cm^2 and 2.75×10^{-3} g/cm^2, respectively. Additional results from the *ORCHID* simulation are shown in Fig. 25.14, with each frame showing the condition of the mesh at different times during the implosion.

The last frame in Fig. 25.14 corresponds to the point in the simulation when the neutron yield equals the total experimental yield. In Fig. 25.15, this frame has been magnified and plots of material density contours, areal density contours, and velocity vectors have been added. From Fig. 25.15(a) it can be seen that the shell-fuel interface has undergone serious deformation, exhibiting a 48% peak-to-valley perturbation. Although the density contours in Fig. 25.15(b) show the same behavior, it is encouraging that the entire fuel region has a density in the range of 0.1 to 0.5 g/cm^3. Areal densities are determined by evaluating the integral of ρdR from the center of the pellet out into the corona, as shown in Fig. 25.15(c). Averaging over the fuel region in this graph gives a value of 1.0 to 1.5×10^{-3} g/cm^2 for the fuel $<\rho R>$. This value is in good agreement with the measured value of $2.13 \times 10^{-3} \pm 3.29 \times 10^{-4}$ g/cm^2 and the one-dimensional result of 1.21×10^{-3} g/cm^2.

The implosion deformations have affected the shell region more seriously. This is especially evident along the polar axis, where – compared with the region along the equator, as shown in Fig. 25.15(b) – significant thinning has occurred. Because of the large variations in density, contributions to the shell $<\rho\Delta R>$ show strong angular dependence. As can be seen in the shell region of Fig. 25.15(c), the integrated values of shell $<\rho\Delta R>$ vary between 5.0×10^{-4} and 3.0×10^{-3} g/cm^2. The average value of 2.12×10^{-3} g/cm^2 is 60%

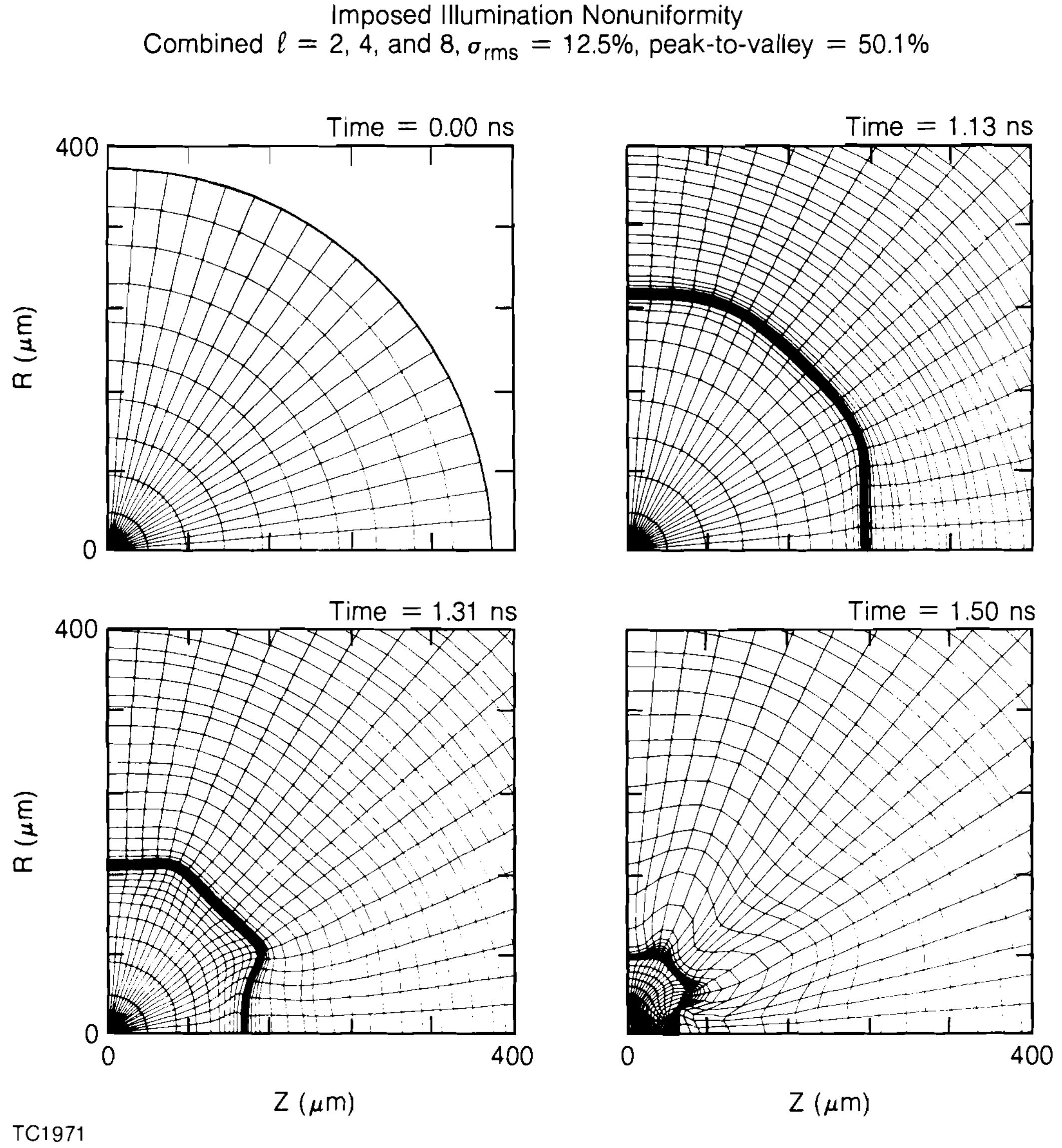

Fig. 25.14
Two-dimensional ORCHID *simulation of shot No. 11233. The imposed illumination nonuniformity was a combined* ℓ = *2, 4, and 8 with a total* σ_{rms} = *12.5%, corresponding to a 50.1% peak-to-valley perturbation.*

higher than the one-dimensional result of 1.31×10^{-3} g/cm^2. There was no shell $<\rho\Delta R>$ measurement taken for this experiment. The comparison between the one- and two-dimensional results indicates that distorted shells can give higher values of shell $<\rho\Delta R>$ than can the one-dimensional predictions.

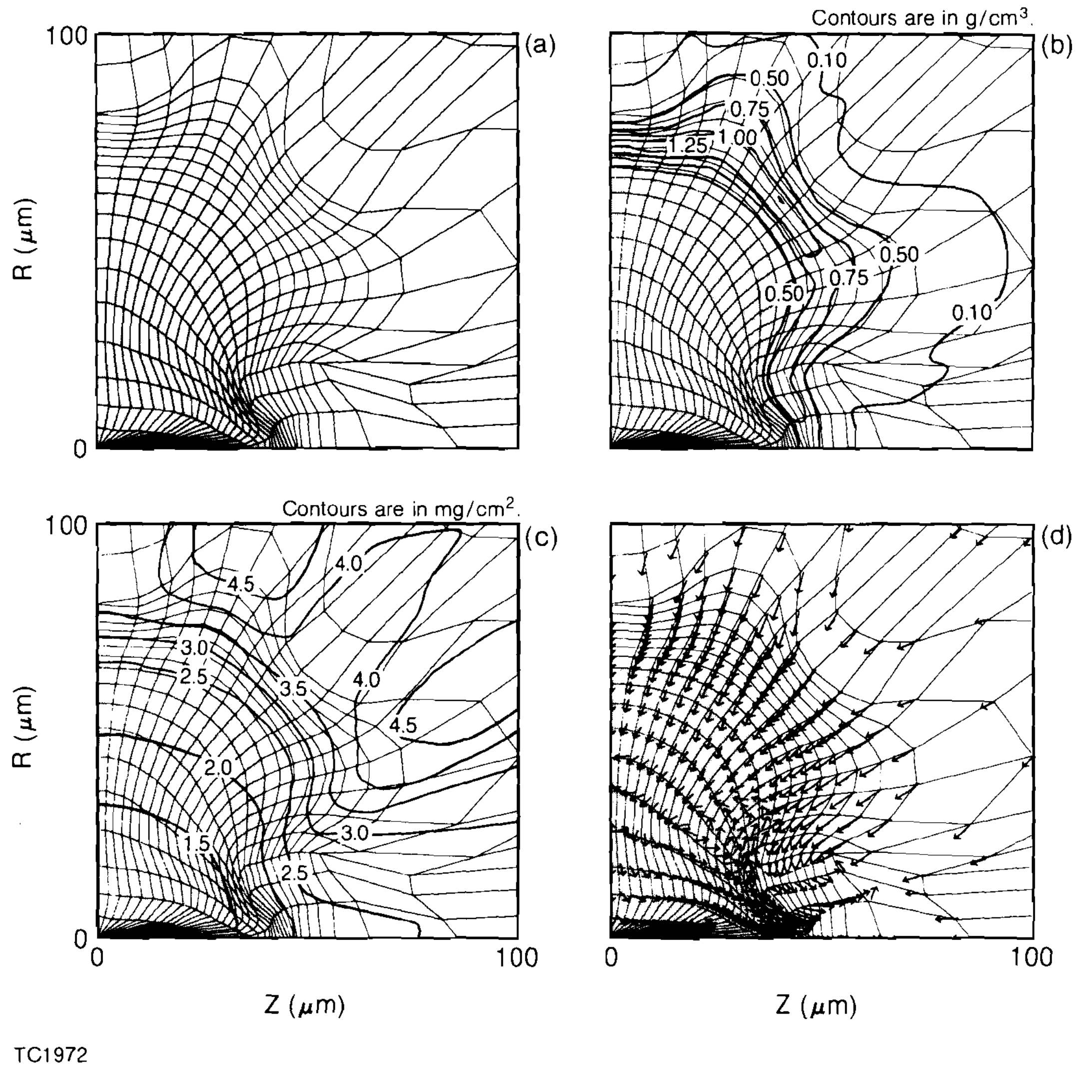

Fig. 25.15
Two-dimensional ORCHID *simulation of shot No. 11233 at 1.50 ns into the simulation:*
(a) grid plot,
(b) material density contours,
(c) areal density contours, and
(d) velocity vector plot.

Finally, in viewing the plot of velocity vectors shown in Fig. 25.15(d), one notes that there is significant fluid motion within the core, especially near the shell-fuel interface along the polar axis. Because the implosion deformations have moved the shell-fuel interface in this area deep into the target, it can be seen that, if mixing processes are present, the swirling fluid motion will transport high-Z impurities from the shell right into the center of the target. The presence of these impurities will seriously affect the core temperature and will possibly quench the burn. Future work on mixing (atomic, chunk, etc.) is needed to determine its effect on overall target performance.

Conclusion

There appears to be agreement between experiment and one-dimensional simulations up to a time prior to maximum compression. After this point in the experiment, however, comparisons between the experiment and one-dimensional simulations show declining agreement as the predicted convergence ratio increases. The mechanism for this behavior is not yet understood but is probably dominated by nonuniformities imposed on the target during the implosion. Two-dimensional simulations have been carried out with the applied levels of nonuniformities predicted for the OMEGA system and have shown less degradation in target performance than that obtained between experiments and one-dimensional simulations. The two-dimensional work has indicated, however, the need for studying the effects of the glass shell mixing in with the fuel. The severe shell distortions caused by the implosion nonuniformities allow mixing processes (atomic, chunk, etc.) to be able to introduce high-Z impurities deep within the hot fuel core, which would seriously degrade the burn. To what extent the mixing processes are able to affect target performance is dependent on the shape and magnitude of the deformations. Future experiments, therefore, will begin to reproduce increasingly larger percentages of one-dimensional predictions, as problems with illumination uniformity on the OMEGA system are identified and corrected.

ACKNOWLEDGMENT

This work was supported by the U.S. Department of Energy Office of Inertial Fusion under agreement No. DE-FC08-85DP40200 and by the Laser Fusion Feasibility Project at the Laboratory for Laser Energetics, which has the following sponsors: Empire State Electric Energy Research Corporation, General Electric Company, New York State Energy Research and Development Authority, Ontario Hydro, Southern California Edison Company, and the University of Rochester. Such support does not imply endorsement of the content by any of the above parties.

REFERENCES

1. S. Kacenjar, S. Skupsky, A. Entenberg, L. Goldman, and M. Richardson, *Phys. Rev. Lett.* **49**, 463 (1982).
2. E. M. Campbell, W. M. Ploeger, P. H. Lee, and S. M. Lane, *Appl. Phys. Lett.* **36**, 965 (1980).
3. H. Brysk, *Plasma Phys.* **15**, 611 (1973).
4. M. C. Richardson, R. S. Marjoribanks, S. A. Letzring, J. M. Forsyth, and D. M. Villeneuve, *IEEE J. Quantum Electron.* **19**, 1861 (1983).
5. University of Rochester, LLE Report 16 (1976).
6. B. I. Bennett, J. D. Johnson, G. I. Kerley, and G. T. Rood, Los Alamos National Laboratory Report LA-7130 (1978).
7. R. C. Malone, R. L. McCrory, and R. L. Morse, *Phys. Rev. Lett.* **34**, 721 (1975).
8. W. F. Huebner, A. L. Merts, N. H. Magee, and M. F. Argo, Los Alamos National Laboratory Report LA-6760-M (1977).
9. M. Born and E. Wolf, *Principles of Optics* (Pergamon, New York, 1975), p. 123.
10. P. W. McKenty and C. P. Verdon, LLE Theory Group Report No. 15 (1985).
11. LLE Review **24**, 61 (1985).
12. S. Skupsky and K. Lee, *J. Appl. Phys.* **54**, 3662 (1983).